

# The infrared reflection nebula around the embedded sources in S 140

David Harker<sup>1,2</sup>, Jesse Bregman<sup>2</sup>, AGGM Tielens<sup>2</sup>, Pasquale Temi<sup>1</sup>, and David Rank<sup>1</sup>

<sup>1</sup> University of California Observatories/Lick Observatory University of California, Santa Cruz, CA 95064, USA

<sup>2</sup> NASA Ames Research Center, MS 245-6, Moffet Field, CA 94035-1000, USA

Received 6 October 1995 / Accepted 23 July 1996

**Abstract.** We have observed the protostellar system in S 140 at 2.2, 3.1 and 3.45  $\mu\text{m}$  using a 128x128 InSb array camera with the Lick Observatory 3m telescope. We have developed a simple model of this region which has been used to derive the physical conditions of the dust and gas. IRS1 is surrounded by a dense dusty disk viewed almost edge-on. Photons leaking out through the poles of the disk illuminate the inner edge of a surrounding shell of molecular gas as seen at locations NW and VLA4. The optical depth at K through the poles of the disk is about 0.22, while  $A_V=30$  towards IRS1. Analysis of the observed colors and intensities of the NIR light, using Mie scattering theory, reveals that the dust grains in the molecular cloud are somewhat larger than in the general diffuse interstellar medium. Moreover, the incident light has a “cool” color temperature,  $\simeq 850-900\text{K}$ , and likely originates from a dust photosphere close to the protostar. There is little  $\text{H}_2\text{O}$  ice associated with the dusty disk around IRS1. Most of the 3.1  $\mu\text{m}$  ice extinction arises instead from cool intervening molecular cloud material. We have also compared our infrared dust observations with millimeter and radio observations of molecular gas associated with this region. The large scale structure observable in the molecular gas is indicative of the interaction between the protostellar wind and the surrounding molecular cloud rather than the geometry of the protostellar disk. We conclude that S 140 is a young blister formed by this outflow on the side of a molecular cloud and viewed edge-on.

**Key words:** ISM: S 140 – stars: S 140 IRS 1 – reflection nebulae – dust – infrared: ISM: continuum; lines and bands

## 1. Introduction

Stars in the early stages of formation are deeply embedded within dense molecular clouds, making it impossible to study them at visible wavelengths. However, the extinction in the infrared is low enough that many protostellar objects and their surrounding environments can be studied. In this paper we report observations and model the infrared emission from the embedded source IRS1 in S 140, which is either a protostar or

a YSO surrounded by a dense envelope (Harvey et al. 1978). We do not distinguish between these phases of stellar evolution here, and for convenience will refer to the embedded sources as protostellar objects.

The current model for a protostellar object (Downes et al. 1981) consists of a protostar surrounded by a dense dusty disk of material. As part of the cloud collapses to form the protostar, the surrounding material collapses into a disk due to the conservation of angular momentum. Mass loss from the star is channeled by the disk into a bipolar wind which sweeps out an elongated cavity within the molecular cloud. Photons can then escape more easily along the poles of the disk than through the plane of the disk. Material forming the cavity lobes scatter the photons from the central source toward the observer, thus creating an infrared reflection nebula. Infrared reflection nebulae around protostars have been studied observationally as well as theoretically (Werner et al. 1983, Pendleton et al. 1986, Pendleton et al. 1990).

The molecular cloud in S 140 is a very well studied system and a source within it, IRS1, is a good example of the formation of a high mass star of spectral type B (Beichman et al. 1979, Hackwell et al. 1982, Evans et al. 1989, Hodapp 1994). It lies at a distance of 910 pc (Crampton and Fisher 1974) and several sources have been resolved with mid-infrared (IRS1, 2, 3 and NW) and radio (VLA 4) observations (Beichman et al. 1979, Simon et al. 1983, Harvey et al. 1988). In the near-infrared region the source IRS 2 is not detected while the others are quite strong (Forrest and Shure 1986, Evans et al. 1989). Towards IRS1, absorption by water ice produces a strong 3.1  $\mu\text{m}$  absorption band (Joyce and Simon 1982) with  $\tau_{3.1} = 1.2$ .

IRS1 is the most likely source of illumination for a majority of the infrared reflection nebula in S 140 (Hayashi et al. 1987). Polarization maps at 2.2  $\mu\text{m}$  show that the polarization is centrosymmetric around IRS1 which itself has a polarization of about 13.5% in a 20'' beam. (Dyck and Lonsdale 1979, Lonsdale et al. 1980, Sato et al. 1985, Joyce and Simon 1986). The polarization reaches a maximum value of 43%, 20'' N of IRS1 near IRS2 (Joyce and Simon 1986). While Lonsdale et al. (1980) attribute the polarization towards IRS1 as due to dichroic absorption, the

polarization angle in the 20'' beam centered on IRS1 is the same as that of the features NW and VLA4 suggesting a large scattered light component. High angular resolution (1'') 1  $\mu\text{m}$  polarization and intensity maps (Lenzen 1987) show low polarization at the position of IRS1, with maximum polarization (50-60%) in the lobes to the north and south. Lenzen also concludes, as does Evans et al. (1989), that IRS1 has bipolar outflows which have cleared the material surrounding it, allowing NIR photons to escape and scatter off the dense dust regions VLA 4 and NW, which show high polarization. Evans et al. claim that radio emissions observed from these two dust regions result from shocks created by the interaction of the stellar wind and the surrounding dense material.

Although IRS1 and 3 both have low 2.2  $\mu\text{m}$  polarization and emission at 20  $\mu\text{m}$ , indicating they are self-luminous, their NIR colors are not consistent with reddened stars (Evans et al. 1989). Evans et al. (1989) conclude that IRS1 is the result of emissions from dust grains with a temperature range between 1000 and 2000 K, inferring a reddening of  $E_{H-K} \sim 1.4$ , and  $A_V \sim 23$  mag. The luminosity of IRS1 between 1.2-4.8  $\mu\text{m}$  is  $\sim 1.6 \times 10^3 L_\odot$ , which is 10-30% of the total luminosity of  $5 \times 10^3 L_\odot$  (Lester et al. 1986). Assuming the grains are at thermal equilibrium, Evans et al. (1989) predict that a large amount exists close to IRS1 ( $\sim 10^{14}$  cm). However, the extended ( $\sim 5''$ ) optically thin HII region observed in radio observations, shows that ionizing photons escape in some directions. Hence, this suggests that IRS1 is surrounded by a dusty disk which may be involved in collimation of the bipolar outflows (Evans et al. 1989).

High velocity outflows were first observed by Blair et al. (1972) in CO maps. Blue and redshifted CO outflows were found to be centered on IRS1 and overlapped with only a 35'' separation, prompting the conclusion that the disk around IRS1 is being viewed almost pole on (Sato et al. 1985, Joyce and Simon 1986, Hayashi et al. 1987). Hayashi et al. (1987) also found the flows to have an anisotropic intensity with the blue shifted flow 3 times more massive than the redshifted flow and elongated to the north of the molecular cloud. They measured the axis of the flows through IRS1 to be at an angle  $\approx -20^\circ$  ( $0^\circ$  being north), perpendicular to the IR polarization of about  $60^\circ - 80^\circ$ .

Large scale radio observations of CS and NH<sub>3</sub> show a ridge or part of a gaseous ring around the protostellar sources (Hayashi and Murata 1992, Zhou et al. 1993). The highest concentration of gas lies to the south of IRS1 along the feature VLA4. To the north, part of the "ring" is missing, and it appears that the CO outflows extend through this gap (Hayashi and Murata 1992).

Finally, studies of HCO<sup>+</sup> emission (Wilner and Welch 1994) indicate that the dusty disk around IRS1 is not pole on, but almost edge-on with an inclination angle  $\leq 20^\circ$ .

In this paper we present observation and analysis of 2.2, 3.1, and 3.45  $\mu\text{m}$  images of S 140. Section 2 discusses the observations. Section 3 describes the data analysis and results, including a discussion of the scattering model. In Sect. 4 we present the discussion of the results, and in Sect. 5 we summarize our conclusions.

## 2. Observations

The observations were made from the Lick Observatory 3 m telescope on Mt. Hamilton on 19 September, 1992. An infrared camera was used with a 128x128 InSb array manufactured by Amber Engineering. The InSb detector was operated at pumped LN<sub>2</sub> temperatures. Broadband anti-reflection coated lens, filter, and window assemblies are optimized for the 2-3  $\mu\text{m}$  wavelength region. The camera has a filter wheel holding 6 fixed filters, a 38mm f/1.5 ZnSe reimaging lens (operating at a focal reduction of 2), with field and Lyot stop baffles. The plate scale is 0.32 arcsec per pixel.

The data were obtained in a staring mode through the three different filters, with integration times ranging from 30 sec at K to 5 sec at 3.45  $\mu\text{m}$ . Total on source times were 120 seconds at K, 720 seconds at 3.1  $\mu\text{m}$ , and 72 seconds at 3.45  $\mu\text{m}$ . The K band filter measures a range of 2.05-2.45  $\mu\text{m}$ , the ice band filter centers at 3.09  $\mu\text{m}$  with  $\Delta\lambda/\lambda = 1.9\%$ , and the 3.45  $\mu\text{m}$  filter has a  $\Delta\lambda/\lambda = 3\%$ . First the object was observed, then the telescope was moved 50 arcsec east and the sky was measured. The sequence continued with the sky being sampled and then the object. An optical CCD guide camera and a gold coated dichroic beamsplitter were used, allowing for accurate guiding with a computer controlled autoguider during each exposure. To produce the final image, each individual image was first shifted to align the bright central source before they were added together.

Figs. 1a-c show the image of S 140 at 2.2, 3.1, and 3.45  $\mu\text{m}$ . Each image was smoothed with a Gaussian filter with a FWHM of 1.5 pixels. Camera orientation was measured by trailing a star N-S across the array while taking a long integration. The images were rotated ( $2.9^\circ$  east of north) to put N to the top and E to the left. Noise for each image was determined by measuring the standard deviation of a few hundred sky pixels.

## 3. Analysis

All images for each filter were registered using the bright central star as a reference, sky subtracted, and flatfielded using dome flats. Alpha Cygnus, observed immediately before S 140, was used for flux calibration, with fluxes taken from the IRTF observers manual. Maps of the color between K and [3.45] ([3.45] is the magnitude at 3.45  $\mu\text{m}$ ), water ice depth at 3.1  $\mu\text{m}$ , and a scaled intensity at K band were created using mathematical procedures, which are specified below, applied to the original object maps.

The K band image of S 140 (Fig. 1a and annotated in Fig. 1d) clearly shows the features in the nebula. The brightest spot at the center is IRS1 while IRS3, a bright but dimmer feature, lies to the east of IRS1. To the north and south of IRS1 are the NW and VLA4 features respectively. North of NW is the position of IRS2 which, as pointed out by previous investigators, is not seen in any of our NIR images.

To provide quantitative results, we took line cuts starting from IRS1 and extending radially out into the nebula as indicated in Fig. 1d. Hereafter we will refer to the lines as they are labelled

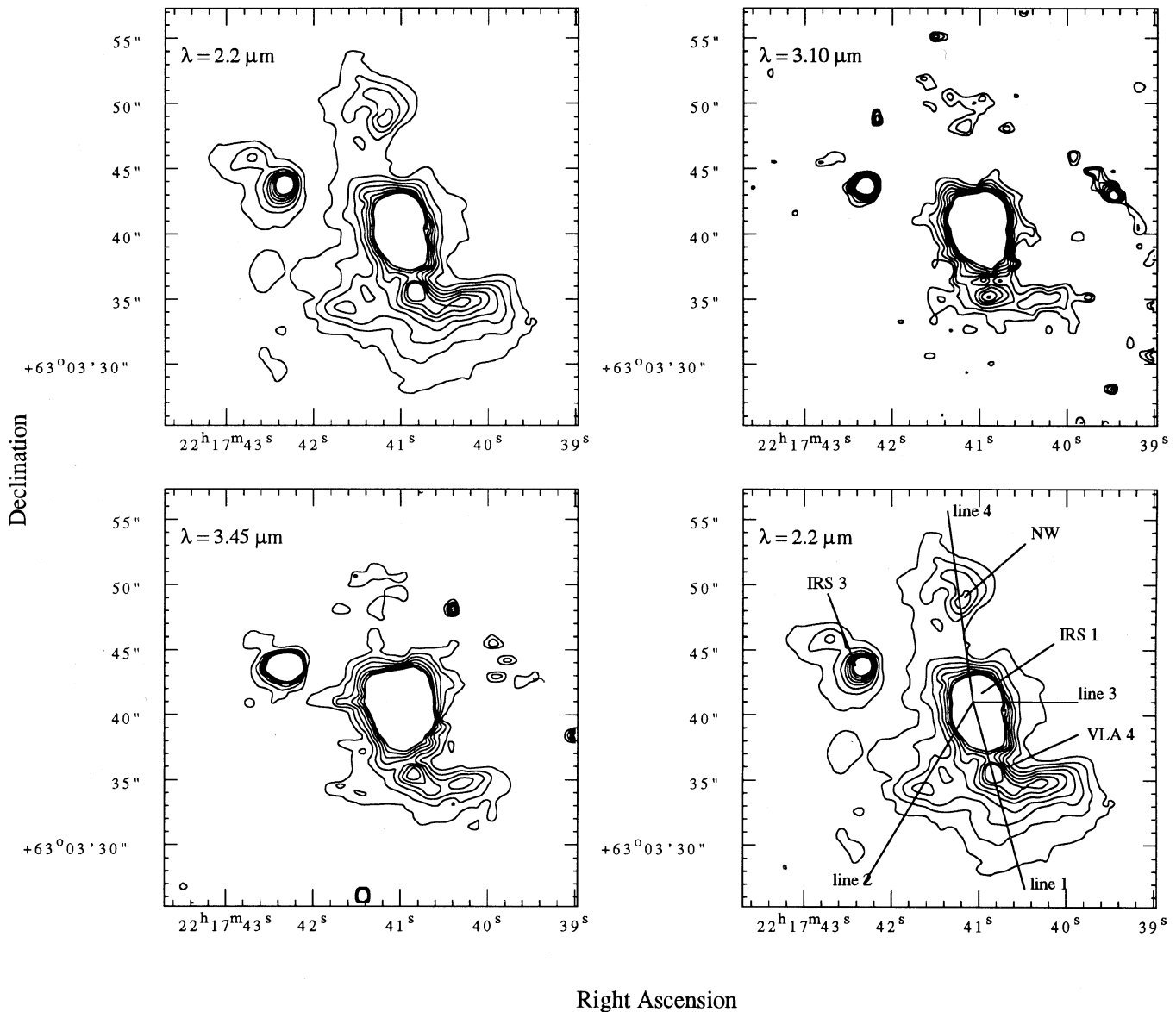


**Fig. 1.** Contour maps of 2.2, 3.1 and 3.45  $\mu\text{m}$ . The lowest contour level for 2.2  $\mu\text{m}$  is  $5.2 \times 10^{-4}$  Jy per pixel, about the  $4\sigma$  level. The lowest contour levels for 3.1 and 3.45  $\mu\text{m}$  are  $9.0 \times 10^{-4}$  and  $2.2 \times 10^{-3}$  Jy respectively, about the  $2\sigma$  level. Contour intervals are  $5.2 \times 10^{-4}$ ,  $1.1 \times 10^{-3}$  and  $1.1 \times 10^{-3}$  Jy for 2.2, 3.1 and 3.45  $\mu\text{m}$  respectively. **d** is the 2.2  $\mu\text{m}$  map annotated with the various sources identified by Beichman et al. (1979), Simon et al. (1983), and Harvey et al. (1988), and the line cuts used in much of the discussion for the paper.

in the figure. The data were averaged over small rectangular apertures (1.28'' wide, 0.64'' along the line direction) to improve the signal-to-noise. Since the  $\text{HCO}^+$  observations (Wilner and Welch 1994) suggest a horizontal disk, the line cuts were taken perpendicular to the disk (lines a and d), along the disk (line c), and in intermediate direction (line b).

In the following sections we will show that the data are best explained by radiation from a central source surrounded by an edge-on dusty disk oriented E-W. The  $\text{HCO}^+$  observations (Wilner and Welch 1994) show that the tilt of the disk is between edge on ( $0^{\circ}$ ) and  $20^{\circ}$ . Since for the model calculations there is little difference between a  $0^{\circ}$  and  $20^{\circ}$  tilt ( $\cos 20^{\circ} = 0.94$ ) we assume for the model an edge-on disk.

### 3.1. Ice depth

Water ice both in the surrounding molecular cloud and in the region around the protostar produces a strong absorption band at 3.1  $\mu\text{m}$ . To produce an ice band optical depth map, the 3.1  $\mu\text{m}$  image was subtracted from an unextincted 3.1  $\mu\text{m}$  image interpolated from the 2.2 and 3.45  $\mu\text{m}$  images. Two methods were used to produce the unextincted 3.1  $\mu\text{m}$  image, a linear interpolation and an interpolation in which we assumed a Rayleigh-Jeans spectrum extincted by dust with a wavelength dependence proportional to  $\lambda^{-1.8}$  (Martin and Whittet 1990). The two methods produced very similar maps. The linear interpolation produces ice optical depth values which are at most 3% greater for loca-

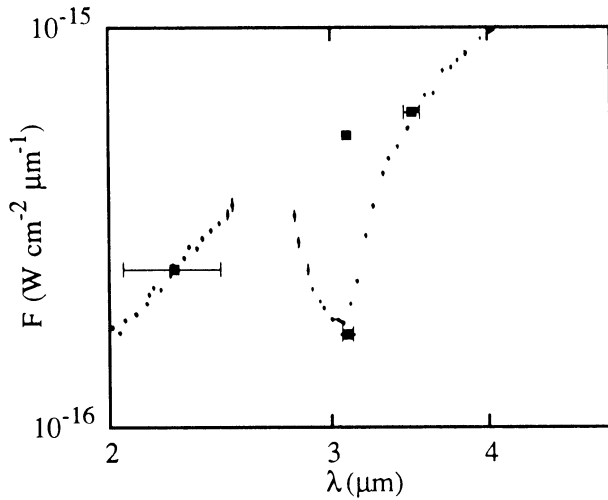


**Fig. 2.** Comparison of the data with spectrophotometric data from Wilner et al. (1982). Plotted above the ice band is the “unextincted”  $3.1 \mu\text{m}$  flux derived from the continuum data. The data have been normalized at K by multiplying our data by 1.25, which accounts for differences in absolute calibration and aperture size and position.

tions in the nebula and 7% less for the point sources than the second method assuming a  $\lambda^{-1.8}$  dependence to the extinction. In the remainder we will use the ice extinction derived using the linear interpolation method. The value we measure for the ice optical depth towards IRS1 in a synthetic aperture  $6.3 \times 7.2''$  is  $\tau = 1.3$ , in good agreement with the value measured spectroscopically (Joyce and Simon 1982). A comparison of our data with the previous spectrophotometric data (Wilner et al. 1982) is shown in Fig. 2.

Fig. 3e shows a contour and gray scale map of the ice optical depth. The position of IRS1 is indicated by a dark plus. The minimum ice optical depth is located  $\sim 1.8''$  to the south-east of IRS1, at the position of a bright reflection nebula visible at  $1 \mu\text{m}$  (Lenzen 1987). Over the central part of the nebula, the ice optical depth is fairly constant at values between 1.0 and 1.2. Towards the south, the ice optical depth slowly increases, then at the bright ridge, VLA4, there is a sharp increase in the optical depth. Similar trends occur towards the east and west, but at positions much closer to IRS1. These data are quantified in the plots of ice optical depth as a function of distance from IRS1 shown in Figs. 3a-d.

If the ice were mixed with dust, then there should be a 1:1 relationship between the ice optical depth and reddening caused by the dust. Figs. 4a-d show the relationship between color (K-[3.45]) and ice optical depth. The data shows that there is no 1:1 correlation and that the ice optical depth and dust reddening are decoupled (at least in the inner part of the nebula). The nearly constant ice optical depth ( $\tau = 1.1$ ) in the direction of the IRS1 region (ie, the bright region between NW and VLA4) implies that the ice grains which produce the ice band are located in the general surrounding molecular cloud through which we view the IRS1 region. There is no obvious trend associated with IRS1 itself, but rather the ice feature appears to be due to absorption

by water ice within the foreground molecular cloud. If water ice is uniformly distributed within the molecular cloud, then the ice optical depth map just reflects the distance through the cloud to the edge of the cavity excavated by the outflow from IRS1. Presumably, the luminous protostar has evaporated the ice in its immediate surroundings, i.e., the dusty disk, and in the cavity to the north and south. The ice optical depth increases much more rapidly in the outer parts of cut 3 (along the disk direction) than along cuts 1,2 or 4. Perhaps the dust temperature in the surrounding molecular cloud drops more rapidly in this direction due to shielding by the disk. The optical depth increase along line 3 indicates a disk with a radius of about  $3''$  ( $2700 \text{ A.U.}$ ). The scale of the disk indicated by the  $\text{HCO}^+$  data is similar to that implied by the infrared data.

From these plots we can estimate the ice and dust density of the molecular cloud. Looking at line 1, we see that outside the cavity in the molecular cloud ( $d_{proj} > 4''$ ) the ice depth rises at a fairly constant rate with distance. A change in ice optical depth of 0.7 corresponds to a distance change of  $4''$ , which for S 140 is  $5.5 \times 10^{16} \text{ cm}$ . Since  $\tau = 1$  corresponds to a column density of  $1 \times 10^{18} \text{ H}_2\text{O molecules/cm}^2$  (Tielens et al. 1991), the amount of ice in a  $5.5 \times 10^{16} \text{ cm}$  column is  $7 \times 10^{17} \text{ H}_2\text{O molecules/cm}^2$ , implying an ice density of  $n = 13 \text{ H}_2\text{O molecules/cm}^3$ . We can use this result to calculate the total gas density and the fraction of oxygen tied up in  $\text{H}_2\text{O}$  ice. We will show later that for S 140  $A_V = 30$ , so  $N_H = 6 \times 10^{22} \text{ cm}^{-2}$ . The ratio of hydrogen to ice is then  $N_H/N_{\text{H}_2\text{O}} = 8.6 \times 10^4$ , so the hydrogen density is  $\rho_H = 1.2 \times 10^6 \text{ H/cm}^3$ . This value agrees with results from radio data, where density measurements range from a few  $\times 10^5$  to a few  $\times 10^6$ . Finally, comparing  $N_H/N_{\text{H}_2\text{O}}$  to the cosmic ratio of hydrogen to oxygen ( $N_H/N_O = 1200$  (Anders and Greene 1989)) we find that the fraction of oxygen that is present in the ice is 1.4%, a value not atypical for luminous protostars.

### 3.2. Colors

Since the nebula is illuminated by a single central source, spectral variations reflect variations in the dust scattering properties within the nebula or variations in dust extinction. The variation in dust extinction may occur either within the nebula, to the location where the light is scattered in our direction, or along the line of sight in front of the nebula. In the remainder, we will generally assume that the dust scattering properties are constant within the nebula but that the dust density or column density may vary from position to position. We will address this assumption further in Sect. 4. We determined the extinction variations using the color variation between K and [3.45].

Fig. 5 shows the K-[3.45] color map for S 140, with larger positive values being redder. The greatest extinction (K-[3.45]=2.0) occurs along the line of sight towards IRS1, with a secondary peak (K-[3.45]=1.7) towards IRS3 which is a somewhat fainter (20% of IRS1) embedded source. Near IRS1, the extinction contours are flattened E-W in the same direction and with a similar size to the  $\text{HCO}^+$  emission measured by Wilner and Welch (1994). To the north and south, the extinction de-

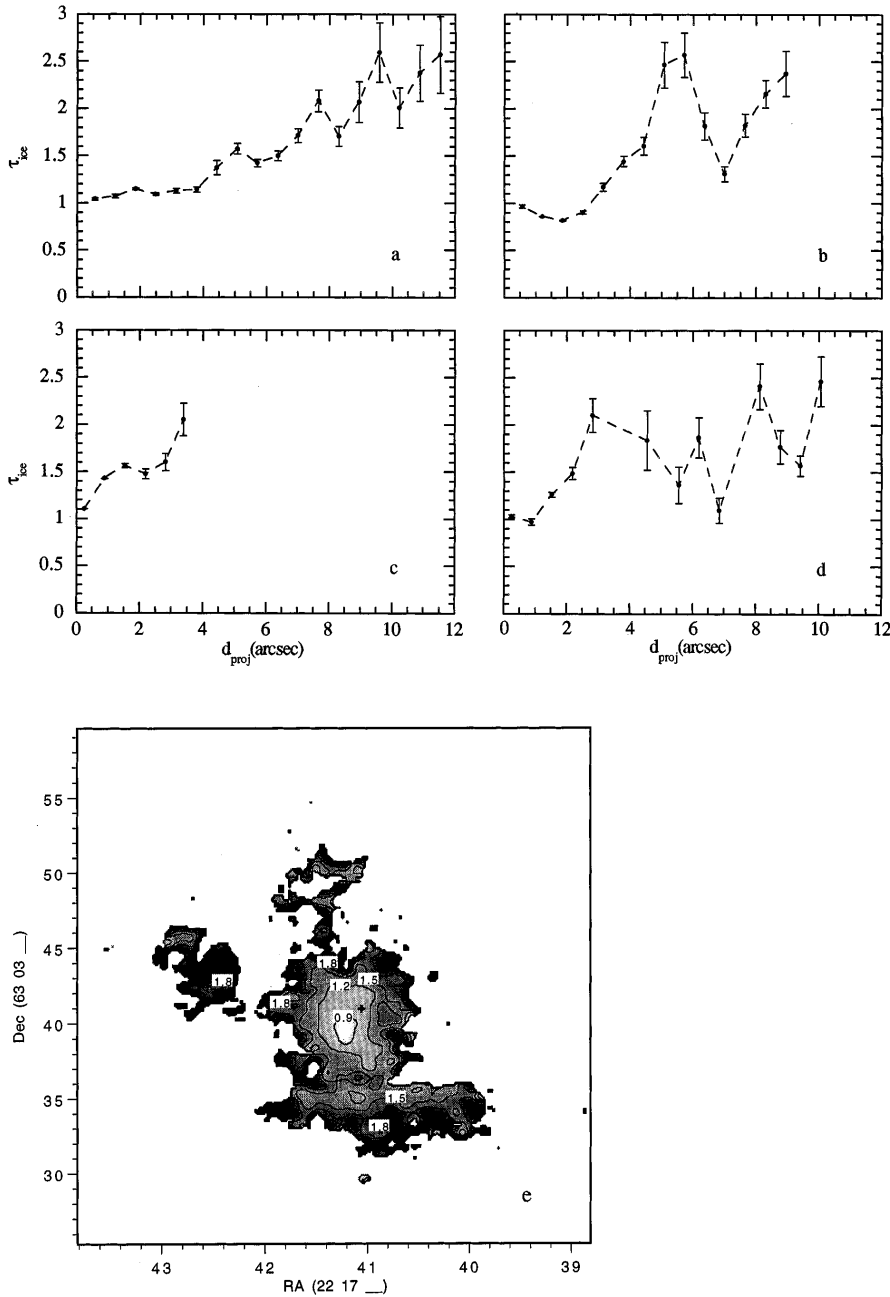


**Fig. 3a–e.** Plots along the four cuts in the nebula (see Fig. 1d) of ice depth ( $\tau_{ice}$ ) versus projected distance (**a–d**) and a contour/gray-scale map of  $\tau_{ice}$ . Plots **a**, **b**, **c** and **d** correspond to cuts 1, 2, 3 and 4 respectively. The dark plus sign in the map shows the location of IRS1.

creases with increasing distance from IRS1 to  $K-[3.45]=-0.3$ , a value representative of the surrounding nebula.

We interpret these results as due to reddening by a dusty disk surrounding the central source. The bright spots are blue because they view the central source along the poles of the disk where the dust is thinnest. Radiation scattered towards us from the cavity/cloud boundary closer to the central source passes through thicker sections of the disk. In Sect. 4.1, we will show that a simple disk model can explain the data. Note that while the flattened  $K-[3.45]$  contours and the  $\text{HCO}^+$  emission are co-aligned with the probable protostellar disk, their size (7000 AU) is on a much larger scale than the disk itself.

### 3.3. Scattering

Following Pendleton et al. (1991), we have modelled the IR reflection nebula to determine the dust scattering properties. To encompass the range of possible models, both the optically thin and optically thick (with low albedo) limits have been explored. If the nebula is illuminated by a dusty photosphere characterized by a color temperature  $T_c$  and a radius  $R$ , a part of the nebula which is at a distance  $d_{neb}$  from the star receives an amount of radiation

$$F = \left( \frac{R}{d_{neb}} \right)^2 B(\lambda, T_c) \quad (1)$$

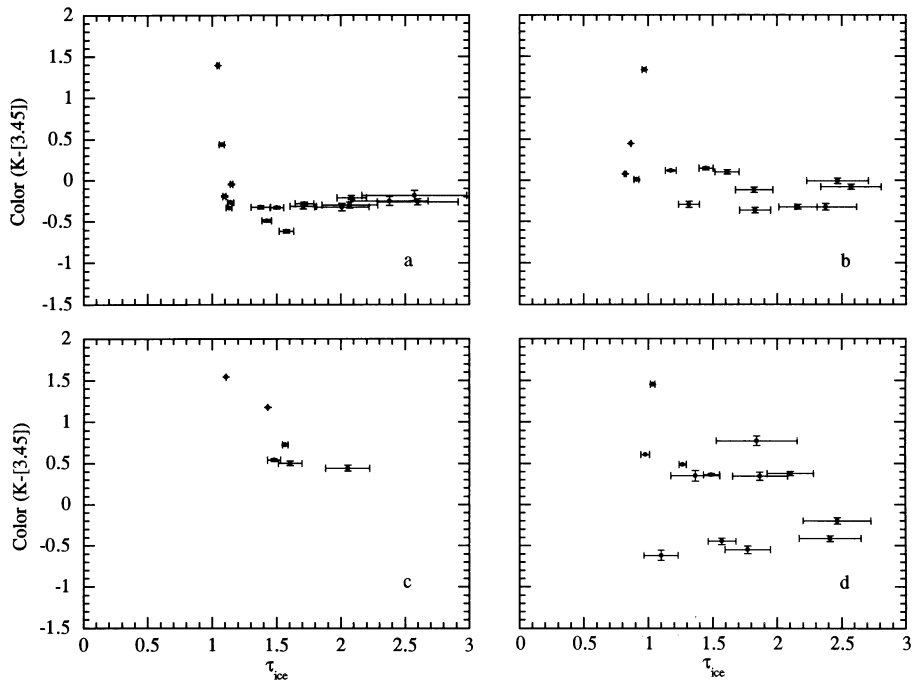


**Fig. 4a–d.** Plots along the four cuts in the nebula (see Fig. 1d) of magnitude difference (or color) between 2.2 and 3.45  $\mu\text{m}$  versus ice depth ( $\tau_{\text{ice}}$ ). Plots a, b, c and d correspond to cuts 1, 2, 3 and 4 respectively.

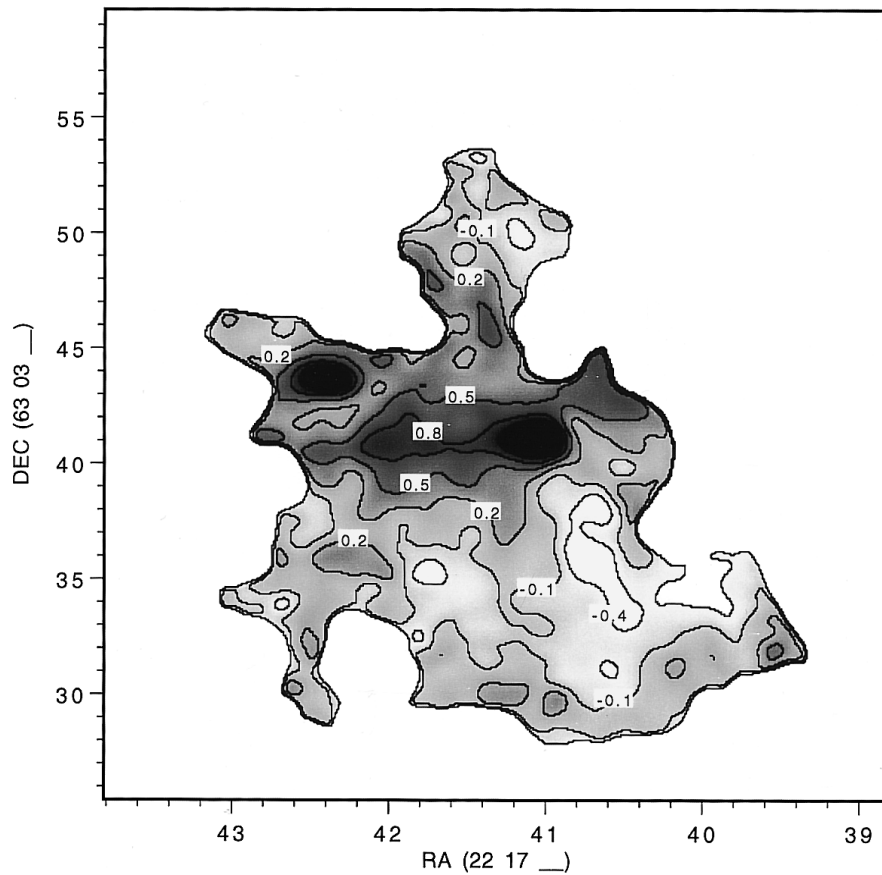


**Fig. 5.** A contour/grayscale map of the magnitude difference (or color) between 2.2 and 3.45  $\mu\text{m}$  ( $K-[3,45]$ ). Larger positive values are redder.

where  $B(\lambda, T_c)$  is Planck's function and we have neglected, for the moment, extinction in the scattering nebula.  $T_c$  is fixed by the observed K-[3.45] color and  $R$  can then be calculated from the known luminosity of the region,  $5 \times 10^3 L_\odot$  (Lester et al. 1986). The scattered intensity into our line of sight in the optically thin limit is then given by

$$I_s = \left( \frac{F\tau_{sca}}{4} \right). \quad (2)$$

where the scattering optical depth  $\tau_{sca}$  along the line of sight is much less than one.

In the optically thick limit, the scattered intensity is determined by the albedo of the particles. For a semi-infinite plane parallel slab the scattered intensity is then given by

$$I_s = F\omega_0 \frac{\mu_0}{4(\mu + \mu_0)}. \quad (3)$$

In Eq. (3),  $\omega_0$  is the albedo and,  $\mu$  and  $\mu_0$  are  $\cos \theta$  and  $\cos \theta_0$  respectively. The angles  $\theta$  and  $\theta_0$  are the angles with respect to the normal of the slab of dust of the outgoing and incoming rays of radiation respectively (Pendleton et al. 1991).

The results for the color ratio (the ratio of flux at two wavelengths), which in this case is  $I_{2.2}/I_{3.45}$ , for small and large scattering optical depths are, respectively

$$\frac{I_{2.2}}{I_{3.45}} = \frac{B(2.2, T_c) \kappa_{sca}(2.2)}{B(3.45, T_c) \kappa_{sca}(3.45)} \quad (4)$$

and

$$\frac{I_{2.2}}{I_{3.45}} = \frac{B(2.2, T_c) \omega_0(2.2)}{B(3.45, T_c) \omega_0(3.45)} \quad (5)$$

where  $\kappa_{sca}$  is the scattering opacity. Equations (4) and (5) show that the ratio of the flux at two wavelengths at a particular position in the nebula is proportional to the ratio of the dust properties (scattering opacity for thin, albedo for thick) at those same wavelengths.

Our observations at 2.2 and 3.45  $\mu\text{m}$  provide us with two relations between four unknowns: the color temperature,  $T_c$ , of the illuminating source, the scattering properties at 2.2 and 3.45  $\mu\text{m}$  and the distance between the central source and the scattering ridge. For the latter we will adopt a distance corresponding to the projected distance, which should introduce an error less than 6% (see Sect. 3). For the scattering properties (i.e.  $\omega_{2.2}$  and  $\omega_{3.45}$ ), we will use Mie scattering calculations for single silicate spheres with size  $a$ . For the scattering angle ( $\mu$  and  $\mu_0$ ) we assume  $\mu = \mu_0$ . We will address the effects of these choices below. We are thus left with two equations (ie. Eqs. 3 and 5 or Eqs. 2 and 4, depending on the optical thickness) in the two unknowns  $T_c$  and the two scattering opacities or albedos at 2.2 and 3.45 which are a function of the grain size  $a$ . The solid line in Fig. 6 represents the unknowns in terms of the color of the nebula (Eq. 5). "Perfect" mirrors at these wavelengths would have an albedo ratio of 1. Small, somewhat hot absorbing grains would have a ratio equal to 3.85, the Rayleigh limit. Typical interstellar grains fall in between these two extremes. The dashed

line is the model prediction for the scattered intensity due to single sized silicate grains using Eq. 3. The intersection of the two curves gives the values for the temperature and albedo ratio which match the observed color for the nebula. From this figure we conclude that the scattering grains radii are typically 1000Å and the color temperature of the illuminating source is  $\simeq 850\text{-}900\text{K}$ . The temperature is in good agreement with the values determined by Evans et al. (1989). Clearly the scattering grains do not "see" the central star but instead see emission from the warm dust grains surrounding the star, as also concluded by Evans et al. (1989). In principle, the presence of dust extinction between the source and the bright ridge would shift the required temperature to higher values. However, much higher temperatures are inconsistent with the high observed intensities and the known luminosity of the region. In Sect. 4.1, our model indicates an optical depth at K of about 0.2 between the source and bright ridge, which would increase the temperature only 30K. This is one of our key conclusions: the high observed brightness at 2.2 and 3.45  $\mu\text{m}$  implies that the peak of the blackbody is well matched to these wavelengths and the grains are efficient scatterers at these wavelengths. This is a very general conclusion which does not depend very much on our assumptions, and is the requirement for producing an infrared reflection nebula. For example, Fig. 6 also shows the relations derived for a size distribution of grains  $n(a)da \propto a^{-3.5}da$  of graphite and silicate grains between  $a_-$  and  $a_+$ . In constraining this set of curves we have varied  $a_-$  from 0.005 to 0.225  $\mu\text{m}$  while conserving the total mass to set the upper limit  $a_+$ . The grain size distribution as predicted by the color is  $a_-$  to  $a_+$  equals 0.02 to 0.34  $\mu\text{m}$ , which is somewhat larger than the MRN distribution (0.005-0.25  $\mu\text{m}$ ) used to model the ISM. Similarly, varying the geometry (i.e.  $\mu_0/(\mu + \mu_0) = 1$ ) does not affect the color ratio but shifts the intensity relation by 50K to a higher temperature.

Using the results for this model we can examine the scattering properties of a larger region of the nebula (i.e. by way of the line cuts (Fig. 1d)). Until this point, we adopted the projected distance (hereafter referred to as  $d_{proj}$ ) from the source IRS1 to the nebula for  $d_{neb}$  in Eq. (1). For this purpose we can calculate  $d_{neb}$  from Eqs. (2) or (3) (depending on which optical depth is being considered), consistent with the observed flux, and hence, the geometry. The ratio  $d_{proj}/d_{neb} = \sqrt{I_{neb}/I_{proj}}$ , where  $I_{neb}$  is the observed surface brightness and  $I_{proj}$  is the surface brightness calculated from Eqs. 1 and 2 assuming the distance from the source to a spot in the nebula is represented by the projected distance, (i.e. the long axis of the nebula is perpendicular to the line of sight). This ratio, which we will call  $S$ , when  $< 1$  is indicative either of extinction within the nebula or an inclination of the nebula to the line of sight. Ratios or values of  $S > 1$  are unphysical. The optically thin case for the grain distribution 0.02-0.34  $\mu\text{m}$  yields a temperature that is insufficient to account for the high intensity seen at 2.2  $\mu\text{m}$  so  $S$  is  $> 1$ . However for the optically thick case,  $S$  is  $< 1$ , so that is the scenario we will use for the rest of the discussion. Note that since  $S$  is a ratio of surface brightnesses, it is independent of the distance to S 140.

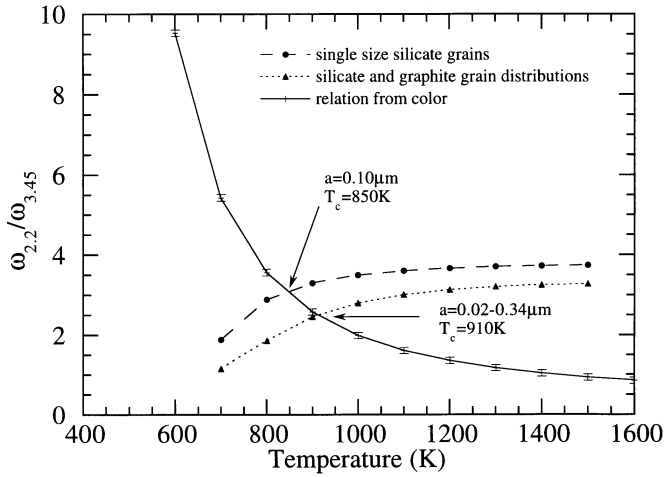


**Fig. 6.** The ratio of albedo at 2.2 and 3.45  $\mu\text{m}$  versus temperature (in K). The solid line represents the relation based on the color of the nebula. The dashed line shows the model prediction for single size silicate grains. The plots intersect where the grain size is 0.1  $\mu\text{m}$  and the temperature is 850K (as noted in the figure). The dotted line is the model prediction for a varying silicate and graphite grain size distribution (in which total dust mass is conserved). The intersection point is at 910K with a size distribution of 0.02-0.34  $\mu\text{m}$ .

## 4. Discussion

### 4.1. Protostar geometry

Figs. 7a-d show  $S$  versus projected distance for the four cuts shown in Fig. 1d. For lines 2, 3 and 4, the  $S$  is nearly constant with distance close to IRS1, then generally increases with distance for lines 2 and 4. For line 3, the surface brightness is too low farther than 4 arcsec from IRS1 to be plotted. Line 1 shows an increase in  $S$  until just past VLA4, followed by a slow decline. Values for  $S$  closer than 1.5 arcsec from IRS1 are dominated by transmitted radiation from IRS1 itself, not by scattering from the dust. We can derive an upper limit to the total extinction between the illuminating source, the bright ridge (near VLA4) and the observer by assuming the ridge is at the projected distance. Since at this point we calculate  $S = 0.82$ , we estimate the maximum amount of extinction in the line of sight to the ridge at 2.2  $\mu\text{m}$  is  $\tau = 0.4$  (i.e.  $S = 1$ ). The decrease in  $S$  towards the central source (Fig. 7a), we interpret as showing increased extinction in a circumstellar dusty “disk”. Hence, the bright ridge is bright because it is located beyond the extinction “shadow” of this disk and because it is right in the path of the relatively unextinguished photons escaping through the poles of the disk density distribution.

To test this hypothesis, we constructed a simple model in which light from the central source, IRS1, shines through a thick disk and scatters off dust at the interface of the evacuated cavity and the molecular cloud (Fig. 8a). The minimum optical depth at K, denoted  $\tau_o$ , corresponds to light escaping through the poles of the disk. By plotting color vs  $1/S$ , the slope of the curves give  $\tau_o$ . The results of the model calculation are compared to the data in Fig. 8b for values of  $\tau_o=0.215$  and 0.26, which are also the

linear least squares fits to the data for lines 2 and 4 (correlation coefficients  $R=0.97$  and 0.92). The optical depth at K for any point along the curves is just  $1/S$  times  $\tau_o$ . The intrinsic color for IRS1 is then the color at  $1/S=0$ , which is  $-0.8$  for both curves, corrected for the albedo difference between K and 3.45  $\mu\text{m}$ . From Fig. 6,  $\omega_{2.2}/\omega_{3.45}$  can range from 2.6-3.0, which results in an intrinsic color for IRS1 of  $+0.3 \pm 0.1$ . Since the observed K-[3.45] for IRS1=1.5, the color excess is 1.2 magnitudes, which gives  $A_K = 2.1$  and  $A_V = 26$  using  $\lambda^{-1.8}$ . Visual absorption can also be calculated from the maximum observed value of  $\tau_K=1.14$  deduced from Fig. 8b ( $1/S=5.3$ ,  $\tau_o=0.215$ ). Since  $A_K = 2.5\tau_K$ ,  $A_K = 2.85$  and  $A_V = 34$ . Thus, we conclude that  $A_V$  is between 26 and 34. Evans et al. (1989) estimate  $A_V=23$  based on a color temperature of about 1000K for IRS1 and observed H and K colors. They calculated a color temperature, and hence intrinsic colors for IRS1, based on the K magnitude of IRS1. An error of 100K in their assumed temperature changes  $A_V$  by 6 magnitudes. From the ratio of the  $Br\gamma$  and  $Br\alpha$  lines, they calculate  $A_V=33$ . Thus, considering the errors, all the results are in good agreement, with a best value for  $A_V$  of  $30 \pm 4$ .

From the model we have derived for S 140, we expect that the scattering angle should increase with increasing distance from IRS1. This would be observable as an increase in the level of linear polarization with distance from IRS1. Existing polarization data at 1  $\mu\text{m}$  shows such a trend (Lenzen 1987), while 2.2  $\mu\text{m}$  polarization maps (Joyce and Simon 1986) show a similar trend but lack the spatial resolution required for a meaningful comparison.

### 4.2. Relationship of protostar to surrounding cloud

The geometry of the region derived from this study consists of a protostar surrounded by a thick dusty disk oriented almost perpendicular to the line of sight. The IR photons escaping through the disk poles set the environment. Recent observations of  $\text{HCO}^+$  (Wilner and Welch, 1994), which shows an extended “disk-like” object centered on IRS1 (Fig. 9d), supports the model we have derived for S 140. The  $\text{HCO}^+$  data, with a spatial resolution of  $5''$ , reflects the distribution of the highest density material in the region. The elongation of the disk implies that it is tilted between edge-on and  $20^\circ$  to our line of sight.

Radio observations (CO, CS, CI and  $\text{NH}_3$ ) of S 140 (Figs. 9a-c) show structure on a much larger scale than the 20 arcsec extent of the protostellar region. Both the CS and  $\text{NH}_3$  emission form part of a V-shaped ring which is closed to the south of IRS1 and opened to the north (Fig. 9a) (Hayashi et al. 1992, Zhou et al. 1993). Hayashi et al. (1992) suggest that the observed CS “ring” is in the plane of the sky and is a remnant of the molecular material that has been swept up by a wind from the protostar IRS1. However, if the “ring” were in the plane of the sky, it would be almost perpendicular to the orientation of the dusty disk around IRS1 and this scenario is untenable. We suggest that the ring represents a limb brightened bubble opened to the north, which has been blown by the protostar. Fig. 9c shows that the southern bright spot in the infrared reflection nebula fits nicely into the southern edge of the CS “ring”; that is, this bright

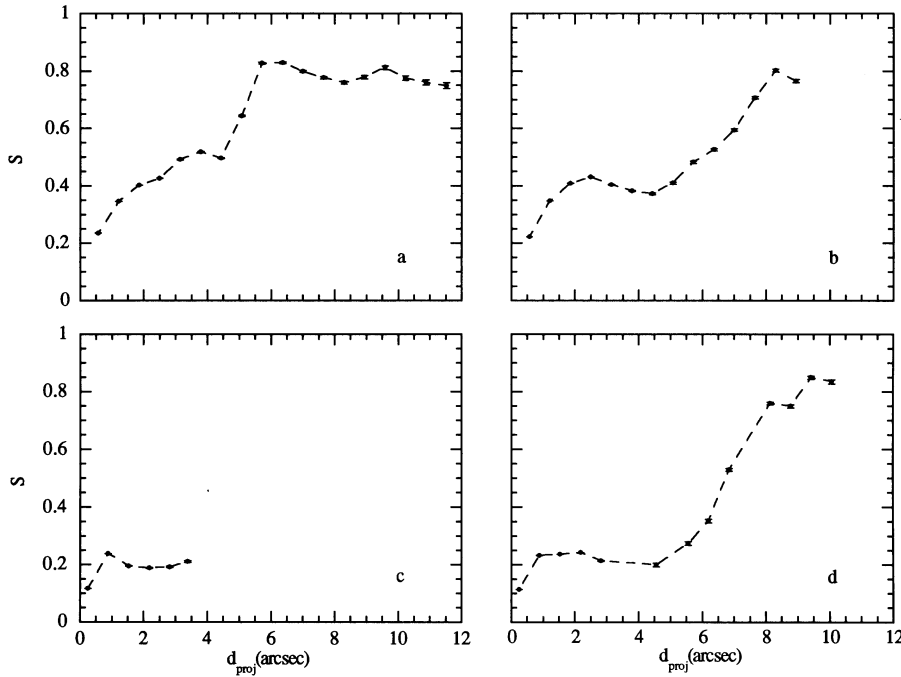


**Fig. 7a–d.** Plots along the four cuts in the nebula (see Fig. 1d) of the ratio of the projected distance and calculated distance ( $S$ ) as determined by the model versus projected distance. Constraints for the model are determined from Fig. 5 with  $T=850\text{K}$  and  $\omega = 0.5$ . Plots **a**, **b**, **c** and **d** correspond to cuts 1, 2, 3 and 4 respectively.

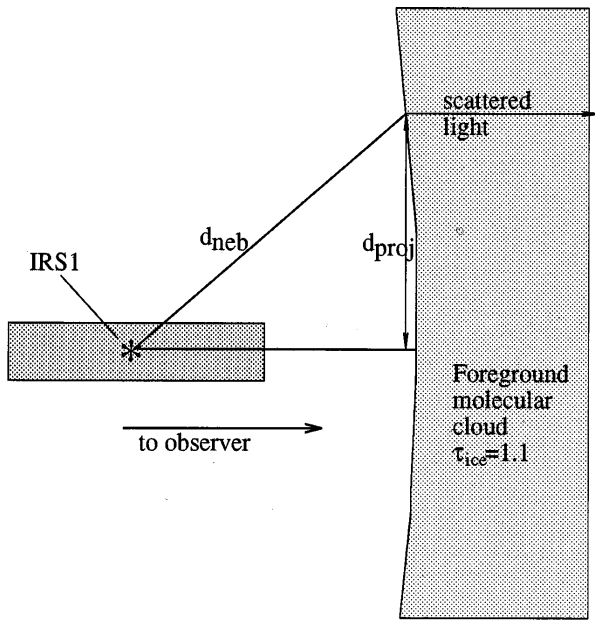


**Fig. 8. a** A schematic of the model used to calculate the  $K-[3.45]$  color as a function of  $S$  ( $d_{proj}/d_{neb}$ ). The results are plotted as dashed lines in Fig. 8b.

spot is the illuminated part of the CS “ring”. This is also where any outflow from the protostar would impact the “ring”.

This disk outflow is in stark contrast to the conclusion discussed in Sect. 1 based on the CO data. We surmise that the red and blue shifted CO peaks are not associated directly with the stellar outflow but rather represent a gas jet or entrained molecular cloud material streaming along the inside of the bubble walls, away from the jet working surface. The observed CO

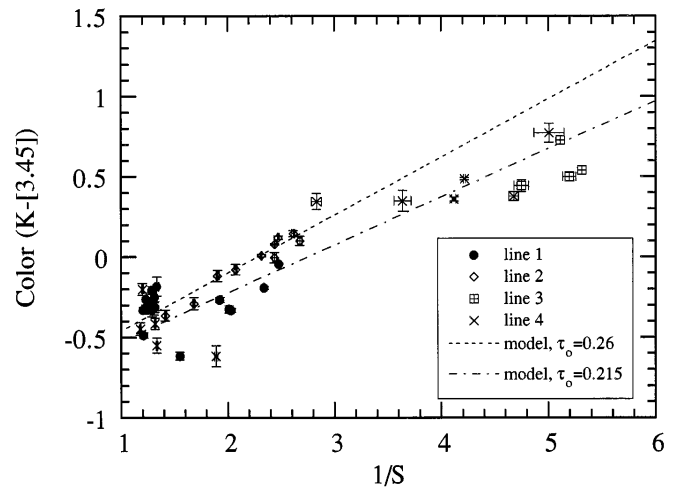


**Fig. 8. b** A comparison of the data for all four line cuts with the results of the model shown in Fig. 8a. The dashed line is the least squares fit to the line 2 data ( $R=0.97$ ) and the dash-dot line is the least squares fit to the line 4 data ( $R=0.92$ ).

morphology then reflects the complex interaction of the stellar jet with the surrounding cloud.

The CO data also show some CO flowing out through the northern gap towards us. It is likely that towards the north the bubble has more or less broken through while in the south it is still confined by the molecular cloud. The geometry of this region resembles that of a blister on a molecular cloud - much like the Orion HII region around the trapezium stars, except for a difference of about  $90^\circ$  in viewing angle. Hence, it seems that stellar outflows can be more important than ionizing photons in shaping the environment of newly formed massive stars,

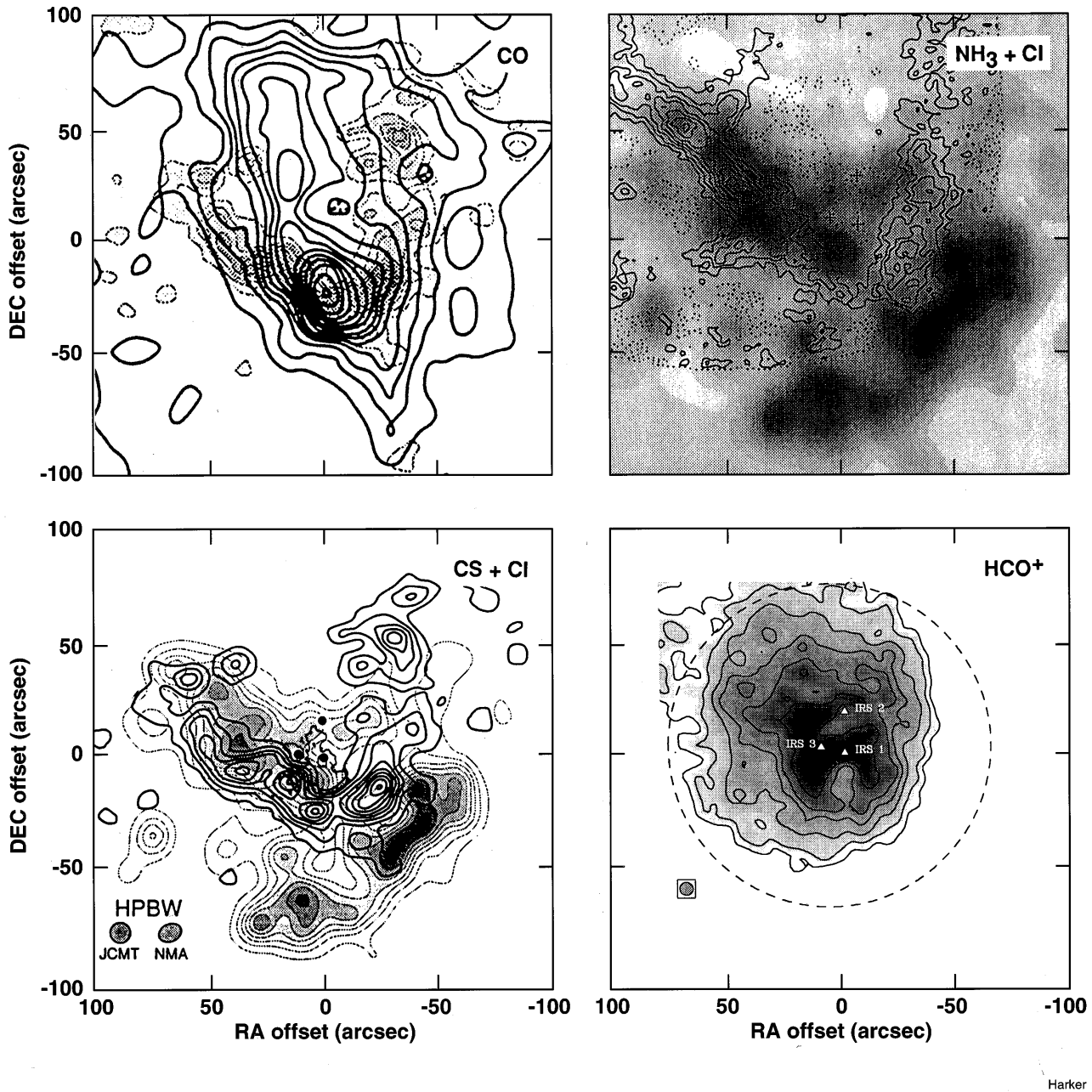


**Fig. 9a–d.** The S140 region on a larger scale. **a** shows the blueshifted CO emission overlaid on the CS (Hayashi et al. 1992). **b** is a plot of the NH<sub>3</sub> contour overlaid on the grayscale CI emission (Zhou et al. 1993). **c** shows the  $4\sigma$  contour level of our K band data overlaid on the CS and CI emission maps (Hayashi et al. 1992). **d** is a grayscale plot of the HCO<sup>+</sup> map.

particularly for regions around B-type stars such as in S 140. This is contrary to much of recent theoretical thinking on such interactions (Yorke 1986). Fig. 10 is a schematic of the S 140 region based on the above observations, taking into account IR and radio data.

Finally, we draw attention to the CI emission observed in the region (Fig. 9b REF). The CI emission observed towards the southeast is due to the photodissociation region associated with the S 140 HII region. The CI emission coincident with the eastern part of the NH<sub>3</sub>/CS “ring” must however have a different

origin. Since the NIR reflection nebula traces the penetration of stellar photons from IRS1 into the cloud, it is clear that IRS1 is not the source of the CO dissociating photons required to produce CI. Mainly based upon location, we suggest that this CI emission originates in a photodissociation region associated with IRS3. This source carries about 20% of the luminosity of this region and is therefore likely a late B-type star. Such stars can cause appreciable CI emission (Spaam et al. 1994). In this picture, the absence of CI emission from the western

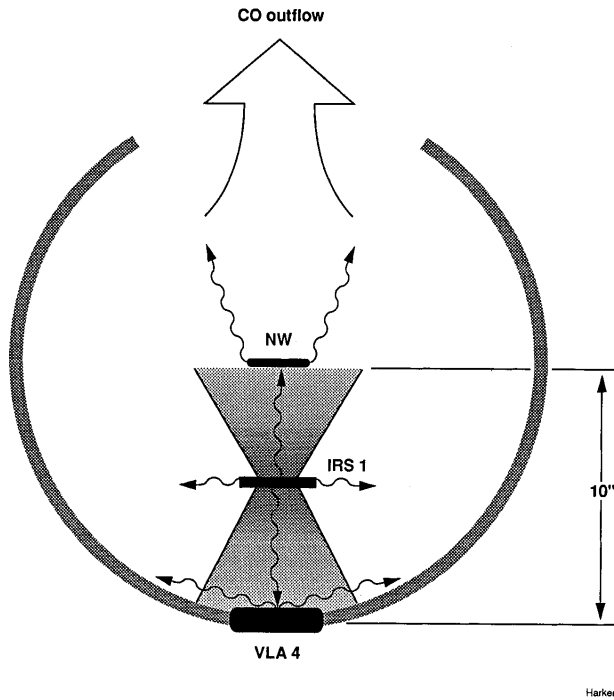


**Fig. 10.** A schematic of the S140 region. Labeled in the figure are the various sources and structures seen in our data and radio observations.

CS/NH<sub>3</sub> “ring” reflects shadowing by the very dusty environment of IRS1.

## 5. Summary

We have observed the molecular cloud S 140 at wavelengths of 2.2, 3.1 and 3.45  $\mu\text{m}$  and have modeled the infrared emission. Our conclusions are as follows:

1. We observed a moderate ( $\tau_{\text{ice}} = 1.1$ ) and nearly constant H<sub>2</sub>O ice depth on and around IRS1. The ice depth steadily increases in the molecular cloud. Hence, there is ice present in the molecular cloud but not in the dusty disk surrounding IRS1. The ice depth observed around IRS1 is due to H<sub>2</sub>O ice present in the foreground cloud. The density of ice in the molecular cloud is  $\rho = 13 \text{ H}_2\text{O molecules/cm}^3$  and the fraction of oxygen present in the ice is 1.4%.

2. Light from the nebula appears to become bluer with increasing distance from IRS1. This observation can be explained if there is a dusty disk around IRS1. Light is reddened by passing through sections of the disk, and the light is bluest along the poles of the disk where the dust is thinnest. The bright southern ridge (VLA4) and the knot to the north (NW) are bright because there is little extinction between them and IRS1 and the dust in these regions is an efficient 2.2  $\mu\text{m}$  scatterer. The trend of K-[3.45] becoming bluer with increasing distance from the central star is a general property of the disk geometry, and should be observable for other protostars with thick disks.

3. A thick disk model can explain both the observed K-[3.45] color and scattered light intensity distributions. The model sug-

gests that the optical depth through the poles of the disk at K is 0.22 and that  $A_V=30$  to IRS1.

4. Observed K-[3.45] colors of the bluest regions implies a cool radiation field with a color temperature of 850-900K. Most likely, these cool temperatures are the result of reprocessing of the protostellar radiation field by dust close to the protostar.

5. The MRN grain distribution, used to model the ISM, cannot explain our observations. A larger grain size distribution (0.02-0.34  $\mu\text{m}$ ) is consistent with the observed color of the nebula, and the geometry of the region.

6. Orientation of the disk around IRS1 is not aligned with the observed CO outflows. The large scale structure observed in the CS, NH<sub>3</sub>, and CO data are indicative of the interaction between the surrounding molecular cloud and the outflows generated by IRS1 rather than the geometry of the region close to the protostar. S 140 is an edge-on blister in the formation phase on the side of a molecular cloud.

## References

- Anders, E., and Grevesse, N. 1989, *Geochim.Cosmochim.Acta*, 53, 197.
- Beichman, C. A., Becklin, E. E., and Wynn-Williams, C. G. 1979, *Ap.J. (Letters)*, 232, L47.
- Blair, G. N., Evans, N. J. II, Vandembout, P.A., and Petters, W. L. III. 1978, *Ap.J.*, 219, 896.
- Crampton, D., and Fisher, W. A. 1974, *Pub.Dom.Ap.Obs.*, 14, 12.
- Downes, D., Genzel, R., Becklin, E. E., and Wynn-Williams, C. G. 1981, *Ap.J.*, 244, 869.
- Draine, B. T., and Lee, H. M., 1984, *Ap.J.*, 285, 89.
- Dyck, H.M. and Lonsdale, C.J., 1979, *A.J.*, 84, 1339.
- Evans, N. J., Mundy, L. G., Kutner, M. L., and DePoy, D. L. 1989, *Ap.J.*, 346, 212.
- Forrest, W. J., and Shure, M.A. 1986, *Ap.J. (Letters)*, 311, L81.
- Hackwell, J.A., Grasdalen, G.L., and Gehrz, R.D. 1982 *Ap.J.*, 252, 250.
- Harvey, P. M., Campbell, M. F., and Hoffman, W. F. 1978, *Ap.J.*, 219, 891.
- Hayashi, M., Omodaka, T., Hasegawa, T. and Suzuki, S. 1985, *Ap.J.*, 288, 170.
- Hayashi, M., Hasegawa, T., Omodaka, T., Hayashi, S. S., and Miyawaki, R. 1987, *Ap.J.*, 312, 327.
- Hayashi, M., and Murata, Y. 1992, *PASJ*, 44, 391.
- Hodapp, K. 1994, *Ap.J.Suppl.*, 94, 615.
- Joyce, R. R., and Simon, T. 1982, *Ap.J.*, 137, 202.
- Joyce, R. R., and Simon, T. 1986, *A.J.*, 91, 113.
- Lada, C. J. 1985, *Ann.Rev.Astr.Ap.*, 23, 267.
- Lenzen, R. 1987, *A.&A.*, 173, 124.
- Lester, D. F., Harvey, P. M., Joy, M., and Ellis, H. B., Jr. 1986, *Ap.J.*, 309, 80.
- Lonsdale, C.J., Dyck, H.M., Capps, R.W., and Wolstencroft, R.D. 1980, *Ap.J. (Letters)*, 238, L31.
- Martin, P.G., and Whittet, D.C.B. 1990, *Ap.J.*, 317, 133.
- Mathis, J. S., Rumpl, W., and Nordsieck, K. H. 1977, *Ap.J.*, 217, 425.
- Pendleton, Y. J., Werner, M.W., Capps, R., and Lester, D. 1986, *Ap.J.*, 311, 360.
- Pendleton, Y. J., Tielens, A. G. G. M., Werner, M. W. 1990, *Ap.J.*, 349, 107.

- Sato, S., Nagata, T., Nakajima, T., Nishida, M., Tanaka, M., and Yamashita, T. 1985, *Ap.J.*, 291, 208.
- Simon, M., Felli, M., Cassar, L., Fischer, J., and Massi, M. 1983, *Ap.J.*, 266, 623.
- Spamms, M., Tielens, A.G.G.M., Van Dishoeck, E., and Bailes, E.L.O. 1994, in preparation.
- Tielens A.G.G.M, Allamandola, L.J., and Sanford, S.A. 1991, in “Solid State Astrophysics”, eds. E. Bussoletti and G. Strazulla, (North Holland Co, Amsterdam), 29.
- Werner, M.W., Dinerstein, H.L., and Capps, R.W. 1993, *Ap.J. (Letters)*, 265, L13.
- White, G.J., and Padman, R. 1991, *Nature*, 354, 511.
- Willner, S. P., Gillett, F. C., Herter, T. L., Jones, B., Krassner, J., Merrill, K. M., Pipher, J. L., Peutter, R. C., Rudy, R. J., Russel, R. W., and Soifer, B. T. 1982, *Ap.J.*, 253, 174.
- Willner, D., and Welch, J. 1993, *Ap.J.*, submitted.
- York, H.M. 1986, *Ann.Rev.Astr.Ap.*, 24, 59.
- Zhou, S., Evans, N. J., II, Mundy, L. G., Kutner, M. L. 1993, *Ap.J.*, 417, 613.